Steel and Composite Structures, *Vol. 21, No. 2 (2016) 411-427*
DOI: http://dx.doi.org/10.12989/scs.2016.21.2.411

Experimental study and modelling of CFRP-confined damaged and undamaged square RC columns under cyclic loading

Li Su [1a], Xiaoran Li [2b] and Yuanfeng Wang [*1]

[1] *Department of Civil Engineering, University of Beijing Jiaotong, No. 3 Shang Yuan Cun, Hai Dian District, Beijing, China*
[2] *Earthquake Engineering Research Center, China Institute of Water Resources and Hydropower Research, Beijing 100038, P.R. China*

(*Received July 21, 2015, Revised March 07, 2016, Accepted April 09, 2016*)

Abstract. While the cyclic behaviour of fiber-reinforced polymer (FRP)-confined columns is studied rather extensively, the cyclic response especially the energy dissipation of FRP-confined damaged and undamaged square RC columns is not yet fully understood. In this paper, an experimental and numerical investigation was conducted to study the cyclic behavior of two different types of Carbon FRP (CFRP)-confined square RC columns: strengthened and repaired. The main variables investigated are initial damage, confinement of CFRP, longitudinal steel reinforcement ratio. The experimental results show that lower initial damage, added confinement with CFRP and longitudinal reinforcement enhance the ductility, energy dissipation capacity and strength of the columns, decrease the stiffness and strength degradation rates of all CFRP-confined square RC columns. Two hysteretic constitutive models were developed for confined damaged and undamaged concrete and cast into the non-linear beam-column fiber-based models in the software Open System for Earthquake Engineering Simulation (OpenSees) to analyze the cyclic behavior of CFRP-confined damaged and undamaged columns. The results of the numerical models are in good agreement with the experiments.

Keywords: reinforced concrete columns; carbon fiber-reinforced polymers (CFRP); cyclic loads; energy dissipation; finite element analysis (FEA)

1. Introduction

Repair and seismic retrofit of concrete columns with fiber-reinforced polymer (FRP) sheets has been widely applied in civil engineering. While the cyclic behavior of FRP-confined RC columns has been studied extensively, a significant amount of research has still been devoted to circular columns retrofitted with Carbon FRP(CFRP), but much less is known about CFRP-confined rectangular/square RC (CFRP-C SRC) columns in which the concrete is non-uniformly confined. Moreover, CFRP-C SRC elements in the existing literature are mainly regarded as the retrofitted specimens. Realfonzo and Napoli (2009) conducted a large-scale experimental program on the CFRP-confined full scale square columns subjected to cyclic loading and evaluated the

*Corresponding author, Professor, E-mail: cyfwang@bjtu.edu.cn
[a] Ph.D. Student, E-mail: su_bjtu@163.com
[b] Ph.D., E-mail: lixiaoran80@126.com

http://www.techno-press.org/?journal=scs&subpage=6 ISSN: 1229-9367 (Print), 1598-6233 (Online)

effectiveness of CFRP in enhancing ductility and energy dissipation capacity of retrofitted columns. Galal *et al*. (2005) evaluated the hysteretic performance enhancement of short RC columns when retrofitted using CFRP. Wu *et al*. (2008) tested three square RC columns externally confined with CFRP and internally inserted small GFRP bars into the concrete. About CFRP stay-in-place formwork, Ozbakkaloglu and Saatcioglu (2007) conducted an experimental investigation on the effectiveness of square CFRP tube for high-strength concrete columns, subjected to simulated seismic loading. Idris and Ozbakkaloglu (2013) also conducted experimental study on seismic behavior of square and circular concrete-filled FRP tube (CFFT) columns, indicating that the FRP tubes significantly enhance the inelastic deformation capacities of the columns. Biskinis and Fardis (2013) proposed two models for the ultimate chord rotation of FRP confined rectangular RC columns based on a large database of cyclic tests. The general conclusion of these studies is that CFRP jacketing is highly effective in strengthen square undamaged RC columns.

Although the confinement effect of CFRP jackets was studied on the non-damaged existing columns, and some useful analytical models were suggested in previous researches for seismic strengthening of square RC columns with CFRP, there is also a need to study the columns which are partially damaged following an earthquake. It can be observed that columns may suffer damage during seismic attacks, therefore, repair of damaged RC members in high-risk seismic zones is frequently necessary. However, a relatively limited number of studies were conducted on the repaired RC members, and existing studies concluded that CFRP jacketing is highly effective for damaged circular, flared or hollow shaped columns (e.g., Xiao and Ma (1997), Sheikh and Yau (2002), Haroun and Elsanadedy (2005), Wang and Li (2013) for circular section; Cheng *et al.* (2003) for hollow section; Saiidi and Cheng (2004) for flared section). Xiao and Ma (1997), Sheikh and Yau (2002), Haroun and Elsanadedy (2005), Cheng *et al*. (2003) and Saiidi and Cheng (2004) conducted experimental researches indicated that the use of FRP significantly enhances the strength, ductility and energy dissipation of the columns. Wang and Li (2013) simulated the cyclic behavior of FRP-confined damaged RC columns and proposed a non-linear damping model for the columns.

Because flexural retrofitting of square or rectangular RC columns by jacketing is less effective due to the poor confinement of concrete in the middle of the column sides, the effectiveness of CFRP for the damaged square RC columns is limited. Saadatmanesh *et al*. (1997) conducted an experimental study on the behavior of two square earthquake-damaged RC columns repaired with CFRP, and found that the strength and ductility of columns with wrapped CFRP is significantly increased. Ye *et al*. (2003) tested two square 200×200 mm RC short columns that a certain damage state was introduced loading the specimens to a predetermined strain level then the specimens were strengthened with wrapped CFRP and tested under lateral cyclic loads. Iacobucci *et al*. (2003) studied seismic repair of two damaged square columns with CFRP, the test results show that added confinement with CFRP enhanced ductility, energy dissipation capacity, and strength of all members. For the damping and dynamic response of FRP-confined circular and square RC columns, Li *et al*. (2014) proposed a stress-dependent damping model for FRP-confined RC material using validated finite element method (FEM) and analyzed the dynamic response of FRP-confined RC columns. Although such studies were all focused on evaluating the effectiveness of using CFRP jackets as a seismic repair technique for columns with different cross-sections, few studies took numerical methods into account as reference (Li *et al*. 2014) to assess the seismic performance of the repaired specimens and conducted comparison with numerical results and test results. It is quite necessary to set up a numerical modeling method to support the study on CFRP-confined damaged rectangular or square RC columns.

The present study evaluates the effects of the initial damage, confinement of CFRP, longitudinal steel reinforcement ratio on the stiffness, strength, ductility and energy dissipation of CFRP-C (D)SRC columns under reversed cyclic load experimentally and theoretically. Results from an experimental program are presented in which 7 columns were tested under constant axial load and cyclic lateral load. For these columns, one is standard RC column, four are strengthened with CFRP before testing, and two columns are tested to a certain damage level, then repaired with CFRP and retested to failure. In order to simulate the cyclic behavior of CFRP-C (D)SRC columns, two hysteretic constitutive models were developed for confined damaged and undamaged concrete and cast into the non-linear beam-column fiber-based models in the software Open System for Earthquake Engineering Simulation (OpenSees). A comparison was made between the results of the numerical models and the experiments.

2. Experimental program

2.1 Specimen details

A total of 9 CFRP-confined square RC specimens were manufactured and tested under lateral cyclic load and simultaneously subjected to constant axial load throughout the test. The specimens were designed as cantilever columns that presented the piers of bridge. Each specimen comprised of a 200×200×2000 mm cantilever column fixed to a 200×300×1500 mm bottom base beam. The height measured from the top of the footing to the applied point of the horizontal force was 1700 mm. The corners of all columns were all rounded with a 20 mm radius to avoid stress concentration of CFRP sheets. Three different longitudinal reinforcement ratios (0.792, 1.553, and 2.567) were considered, consisting of 4Φ10, 4Φ14, and 4Φ18 arrangements. The transverse steel hoops were 6 mm in diameter with yield strength (f_y) of 325 MPa spaced at 100 mm on center. Dimensions and reinforcement details of the test columns are shown in Fig. 1.

Table 1 gives the details of the test specimens. The test specimens were divided into three groups. The first group, column CA, BA5, and CA6, were tested under the as-built condition. Specimen CA was tested to failure to establish a metric behavior for comparison. Specimens BA5

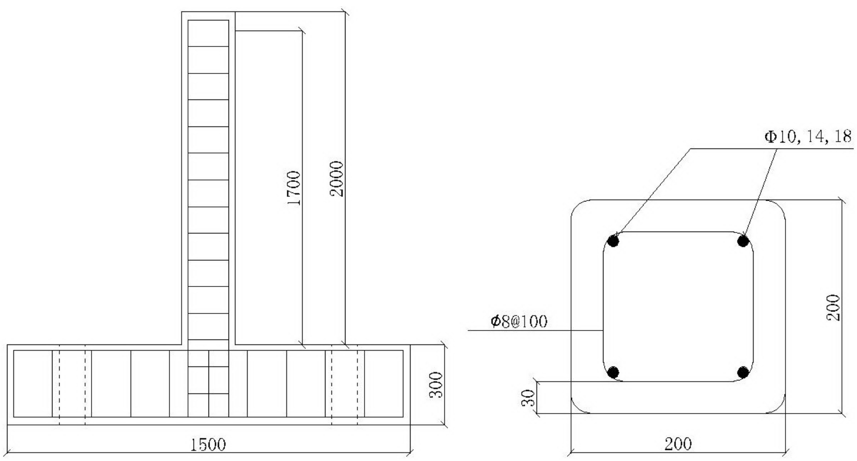

Fig. 1 Geometry and steel configuration of test specimens (unit: mm)

Table 1 Properties of the test specimens

Specimen	Layers of CFRP	Longitudinal steel ratio (%)	Initial fundamental frequency before strengthening (Hz)	Work type	Applied axial compression (kN)	Axial load ratio
AR-1	1	0.792	24.05	Retrofit	185	0.15
AR-3	3	0.792	24.12	Retrofit	185	0.15
BR-1	1	1.553	24.16	Retrofit	200	0.15
BA5	0	1.553	24.21	As-built	200	0.15
BP-1	1	1.553	13.11	Repair	200	0.15
CA	0	2.567	24.53	As-built	220	0.15
CR-1	1	2.567	25.11	Retrofit	220	0.15
CA6	0	2.567	20.59	As-built	220	0.15
CP-1	1	2.567	14.75	Repair	220	0.15

and CA6 were damaged to a certain degree by the end of 5 mm and 6 mm lateral displacement cycles, respectively. The second group, column AR-1, AR-3, BR-1, and CR-1, were strengthened with CFRP before testing. The third group has two specimens, i.e. specimens BA5 and CA6 in group 1 that firstly were loaded to a degree that the columns were still repairable, the specimens were repaired with wrapped CFRP after unloading and renamed as BP-1 and CP-1, and then tested to failure. It should be noted that the first letters "A", "B" and "C" represent the longitudinal reinforcing steel configuration shown in Fig. 1. The second letter, "A" "R" and "P" stand for as-built, retrofitted, and repaired columns, respectively. The number after the horizontal line represents the number of CFRP layers. The main variables studied were the longitudinal reinforcement ratios, the number of CFRP layers, and the level of initial damage.

2.2 Concrete

The test columns were cast with one batch of concrete. Each cast used a ready-mixed concrete design consisting of Type P.042.5R normal portland cement, crushed gravel with a maximum size of 15 mm. The mix proportion of the concrete was: cement/water/sand/limestone/GRACE 1/0.44/ 2.37/2.90/0.014. Development of concrete strength with age was monitored by testing three cubes at one time, and the nominal 28-day mean compressive concrete strength (f_{cu}) is 37.5 MPa.

2.3 Carbon-FRP composite and retrofitting details

The fibers were oriented in the circumferential direction to develop hoop tension. The stress-strain relationship of composite material provided by the manufacturer showed that linear-elastic behavior up to the rupturing tensile strength. Table 2 presents the mechanical properties of the composites. The fiber was wrapped along the whole length of the columns, the overlap length in the circumferential direction and length along the column were both 150 mm. The test coupons were taken from the carbon sheets, impregnated with the same batch of mixed epoxy and cured to harden under the same condition. Install compensatory strain gauges on retrofitted and repaired columns. Each retrofitted specimen was to cure for at least 6 days to ensure full strength gained before testing.

Table 2 Material properties of the CFRP

Material	Material Properties							
	Tensile strength (MPa)	Tensile modulus (MPa)	Elongation (%)	Bending strength (MPa)	Shear strength (MPa)	Specific gravity (g/cm^3)	Breadth (m)	Laminate thickness (mm)
CFRP	4003	2.42×105	1.71	725.7	49.8	1.8	0.5	0.167

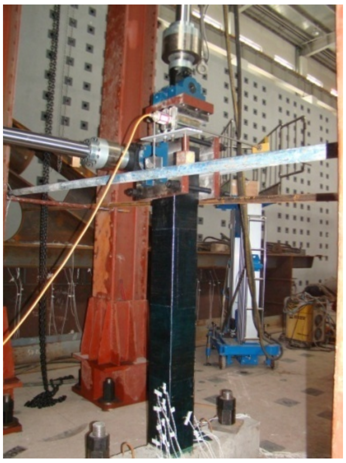

Fig. 2 Details of the test setup

2.4 Test setup and instrumentation

The test setup was designed to subject the columns to a constant axial compressive load and cyclic horizontal linear variable displacement transducers (LVDTs) and strain gauges to measure horizontal, vertic load. The stub was firmly anchored on the ground with two large diameter steel anchor stock. Two 500 kN capacity servo-computer-controlled MTS hydraulic actuators were used to apply the loads. One of the actuators was positioned vertically on the top of the column to apply constant axial compression throughout the test. The other actuator was placed horizontally at the height of the horizontal loading to apply lateral deformation reversals. Fig. 2 illustrates the test setup. The columns were instrumented with al displacements, longitudinal strains in reinforcement and circumferential strains on CFRP sheet of each specimen, as shown in Fig. 2. A total number of 22 strain gauges were placed on the surface of the CFRP, longitudinal reinforcing bars and transverse hoops, respectively. All instrumentations were connected to a data acquisition system and a microcomputer for data recording.

2.5 Loading program

The columns were first subject to axial compression and remain constant. The axial load ratio ($n = N/(f_c(A_g - A_s) + f_yA_s)$) of the test columns was 0.15, where N is the axial load, A_g is the section area of the column, f_c is the compressive strength of concrete, which was calculated by $f_c = 0.76\times f_{cu}$ adopted according to the Chinese concrete structure design code, f_{cu} is the nominal 28-day mean compressive strength of concrete, A_s is the cross section area of the reinforcing bars, and f_y is

Table 3 The lateral displacement amplitude sequence of each specimen

Specimen	Lateral displacement amplitude sequence
AR-1	4 mm, 7 mm, 10 mm, 13 mm, 16 mm, 19 mm, 22 mm
AR-3	5 mm, 10 mm, 15 mm, 20 mm, 23 mm, 26 mm, 29 mm, 32 mm, 35 mm
BR-1	3 mm, 6 mm, 9 mm, 12 mm, 15 mm, 20 mm, 25 mm, 30 mm, 35 mm
BP-1	5 mm, 10 mm, 15 mm, 20 mm, 25 mm, 30 mm, 33 mm, 36 mm, 39 mm
CA	5 mm, 8 mm, 11 mm, 13 mm, 15 mm, 17 mm, 19 mm, 21 mm, 23 mm, 25 mm, 27 mm, 29 mm, 31 mm, 34 mm, 38 mm
CR-1	5 mm, 10 mm, 15 mm, 20 mm, 25 mm, 28 mm, 31 mm, 34 mm, 37 mm, 40 mm
CP-1	4 mm, 8 mm, 12 mm, 16 mm, 20 mm, 24 mm, 28 mm, 32 mm, 36 mm

the yield strength of the steel reinforcing bars. The specimens were then subjected to increasing lateral deformation reversals by using a displacement-control mode of loading. The lateral load sequence consisted of two cycles at each drift ratio, until the specimens were unable to maintain the originally applied axial load. The loading rate is 0.3 mm per minute and remains constant throughout the test. The lateral displacement amplitude sequence of each specimen is shown in Table 3.

3. Test results and discussion

3.1 Test observations

Column CA was cyclically loaded until failure. No visual signs of damage were noticed until the lateral drift displacement reached about 5 mm. It was observed that the first two hairline horizontal cracks occurred at the tension side near the column footing joint when the lateral displacement reached a value of about 8 mm. As the lateral displacement reached a value of 11 mm, the horizontal flexural cracks developed evenly above the first crack and the popping sounds were heard. As the applied lateral displacement increased, additional cracks emerged and developed into flexural-shear cracks. When the lateral displacement was at about 25 mm, the diagonal cracks suddenly opened up and the lateral load reached the peak. When the lateral displacement reached 31 mm, the diagonal crack extended almost from corner to corner, and the concrete began to crush, as shown in Fig. 3. Specimens CA developed an unstable response due to brittle shear failure, and failed at displacement of 38 mm when the column lost its load-carrying capacity of 20%. Specimens BA5 and CA6 were pushed by the end of 5 mm and 6 mm lateral displacement cycles, respectively, and hairline cracks in the bottom concrete covers appeared. For the following investigation of the repaired columns' cyclic behavior, these two columns will be repaired with CFRP after being damaged to a certain level.

In contrast to the as-built columns, the retrofitted samples performed in a consistently stable status throughout the test. Since they exhibited similar behaviors under reversed cyclic loading, specimen AR-1 was selected as a representative sample. There were no apparent damage and sound of epoxy cracking until the lateral drift reached about 7 mm, when an obvious horizontal crack was found. The position of the first crack was near the column-footing interface. As the applied lateral displacement increased, existing horizontal flexural cracks widened and some weak

Fig. 3 The failure of the CA column

(a) AR-1 (b) BR-1

Fig. 4 Views of specimen failures at the end of testing

sounds were noticed. When the second cycle of 10 mm displacement was imposed on the column, the lateral resistance continuously increased to the maximum value as the lateral displacement increased. At this time, the concrete at the compression side near the base crushed and the local fiber rupture occurred at approximately 60 mm from the column-footing interface. Substantial dilation of the concrete and more rupture of fiber within a segment 100-400 mm from the column-footing interface were observed over the last few cycles. The test halted in the 7th cycle at the lateral displacement of 22 mm when the column could no longer support the axial load, and the lateral resistance dropped significantly. The CFRP sheets near the footing were then peeled off from the column for inspection. It was found that the concrete cover in the area between the bottom to 200mm of the column crushed. The failure zone is shown in Fig. 4(a). The failure processes of columns BR-1 and CR-1 are similar to column AR-1, as shown in Fig. 4(b).

Observations made during the testing of the two repaired columns BP-1 and CP-1 were similar to the retrofitted specimens. Compared to the as-built columns, the repaired columns showed very satisfactory performance. It significantly enhanced the ductility and lateral load-carrying capacity, and performed a stable flexural behavior due to more concrete crushing within the plastic hinge zones.

3.2 Hysteretic behavior

Fig. 5 presents the recorded hysteretic load-displacement relationships for each column. All the

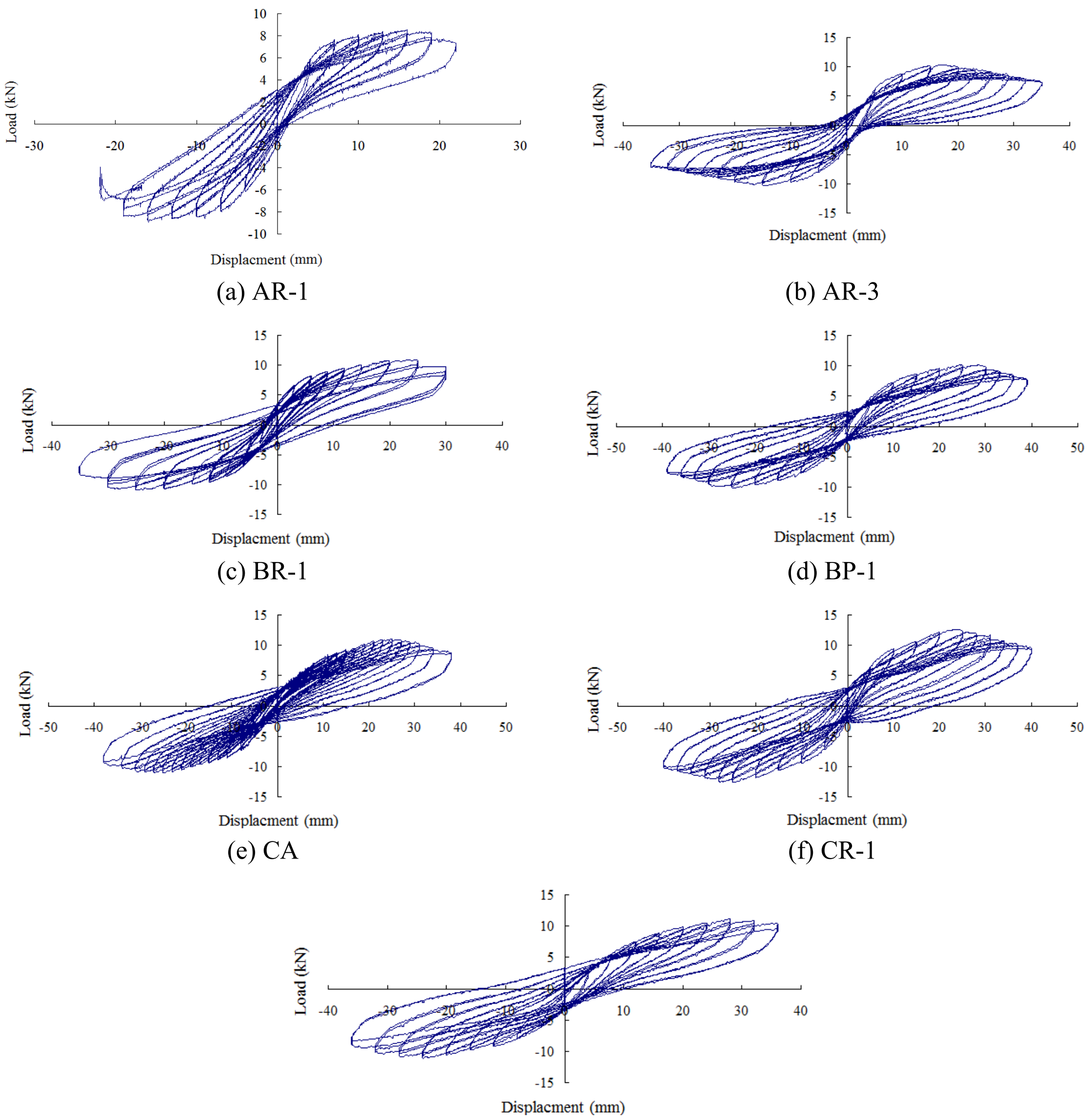

(a) AR-1 (b) AR-3

(c) BR-1 (d) BP-1

(e) CA (f) CR-1

(g) CP-1

Fig. 5 Experimentally recorded hysteretic load-displacement relationships

columns showed a flexure dominant behavior with well-rounded hysteresis loops. Table 4 provides the maximum moments and lateral drift capacities of each specimen. The discussions on the influence of the test parameters investigated in the study on the hysteretic load-displacement relationships are provided in the following sections.

3.2.1 Effect of initial damage

Specimens BP-1 and CP-1 were first tested to a certain level of damage under reversed inelastic cyclic loading before being repaired with one CFRP layer and retested to failure. Envelop curves

Table 4 Observed column behavior

Specimen	f_{cu} (MPa)	Axial load ratio (kN)	Maximum recorded moment (kN·m)	Failure displacement (mm)	Maximum lateral drift (%)
AR-1	37.5	0.15	16.96	22	1.29
AR-3	37.5	0.15	20.70	35	2.06
BR-1	37.5	0.15	21.86	35	2.06
BP-1	37.5	0.15	21.00	39	2.29
CA	37.5	0.15	21.28	38	2.24
CR-1	37.5	0.15	25.46	40	2.35
CP-1	37.5	0.15	22.16	36	2.12

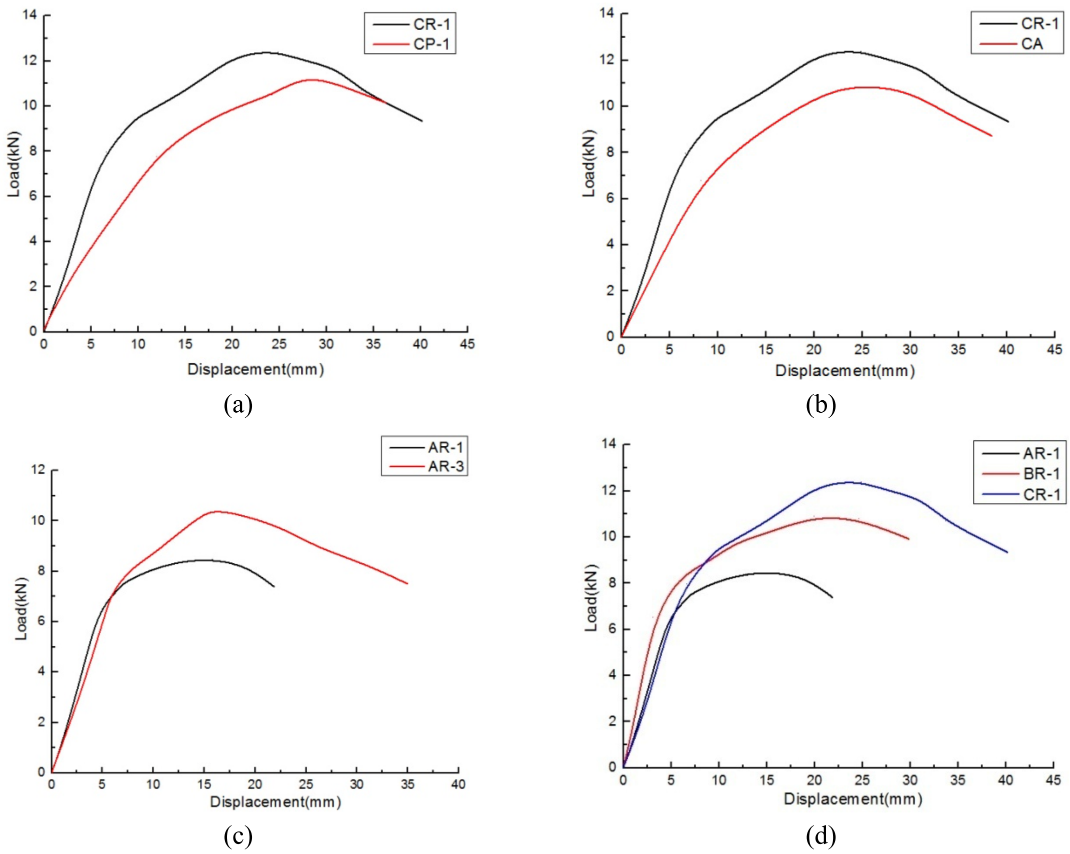

Fig. 6 Comparison of the envelop curves of column lateral load-displacement relationships

presented in Fig. 6(a) show that the behaviors of the repaired columns were resembled to the undamaged wrapped specimens. Nevertheless, it can be seen from Fig. 6 that although the columns BP-1 and CP-1 can also endure larger deformation after being repaired after damage, their initial stiffness was reduced due to cracks and damage before strengthening, and the initial damage of repaired columns resulted in lower displacement ductility than that of retrofitted columns. For example, the ultimate drift displacement of specimens CR-1 and CP-1 were 40.05 mm and 36.05 mm, respectively. The same trend can be found in specimens BR-1 and BP-1, although the first test specimen BR-1 was conservatively applied load, and the test was stopped when it can't fully arrived at its ultimate drift ratio. The increases in the load-carrying capacity of the repaired columns were also relatively low compared with the retrofitted columns. For example, the load-carrying capacity of specimens CP-1 and CR-1 were 11.10 kN and 12.64 kN, respectively, the former dropped about 12.2%, and examination of the shear values of specimens BP-1 and BR-1 indicated that the strengthened specimen's maximum lateral resistance quantity is 7.5% higher than the repaired column. This suggests that previous damage sustained during the cycling of specimens BP-1 and CP-1 are insufficient to fully compensate for the specimens' strength and stiffness.

3.2.2 Effect of the confining CFRP

Fig. 6(b) illustrates that the repaired and retrofitted specimens were seismically superior to the unwrapped column, and their seismic performances progressively improved as the number of CFRP layers increased. The deformation capacity, toughness, and maximum strength values for the as-built column were subordinate to the values for retrofitted specimens. For example, the load-carrying capacity of specimen CA was 11.06 kN, nevertheless, the corresponding value of specimen CR-1 increased to 12.64 kN. It also can be seen that the strengthened specimen CR-1 attained the ultimate displacement quantity 5.61% higher than the unwrapped column, and the strength and stiffness degradations of the wrapped columns were significantly decreased compared with the as-built columns. As shown in Fig. 6(c), the initial stiffness of all the retrofitted columns were generally similar due to that the retrofitting has little effect on the material properties of the concrete at linear elastic stage. However, as the drift ratio increased, an increase in the amount of confining CFRP can result in a significant increase in the ultimate drift ratio and lateral resistance. For example, an additional two layers of CFRP used in specimen AR-3 compared to specimen AR-1 increased the ultimate drift displacement and lateral resistance from 22.03 mm to 25.99 mm and from 8.55 kN to 10.31 kN, respectively. This result reflects that the horizontal confinement of CFRP could effectively enhance the compressive strength and ultimate strain of the core concrete, an increase in the amount of confining CFRP results in an increased plastic hinge length and flexural stable behavior.

3.2.3 Effect of longitudinal reinforcement ratio

The effect of longitudinal reinforcement ratio can be investigated by comparing the behavior of specimens AR-1, BR-1 and CR-1, as shown in Fig. 6(d). These three specimens were all retrofitted with one layer of CFRP. The test results demonstrated that, the ultimate drift displacement of specimens CR-1 and AR-1 corresponding to 80% of the peak lateral load were 34.89 mm and 22.03 mm, respectively, the latter dropped about 36.86%, and the maximum lateral resistance of specimens CR-1 and AR-1 were 12.64 kN and 8.55 kN, respectively, the latter dropped about 32.36%. As the ratio of longitudinal reinforcement increases, the wrapped columns show the enhanced cyclic performance, energy dissipation capacity and decreased rates of the stiffness and strength deterioration. The results may be due to an increase in its drift capacity caused by an increase in the longitudinal reinforcement ratio.

3.3 Energy dissipation

Another important factor for seismic design is the ability of structural element to dissipate

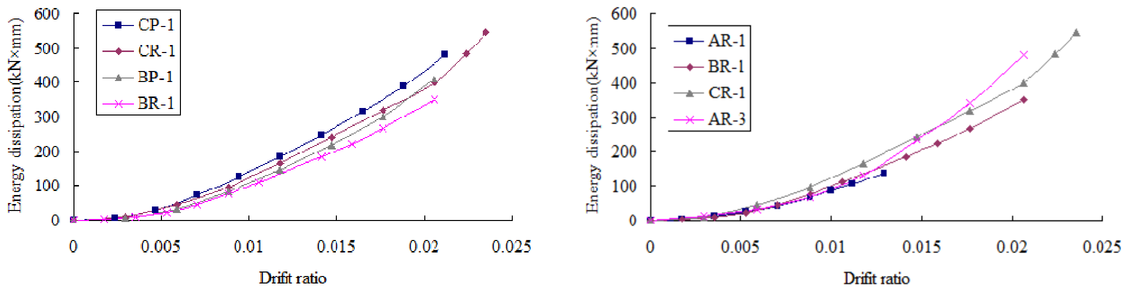

(a) (b)

Fig. 7 Comparison of the dissipated energy versus drift ratio envelopes

energy during an earthquake. In this study, the energy dissipation versus the lateral displacement curves of the specimens were evaluated and given in Fig. 7. The energy dissipated per cycle was calculated from the load-displacement loop, based on the area enclosed by the first cycle of every displacement excursion until the ultimate point was reached. From the figures, we can see that before the lateral displacement reached approximately 0.5% of drift ratio, the energy dissipation of specimens in each set was similar, as the displacement increased further, the energy dissipation of all specimens and the difference among the curves both significantly increased. This demonstrates that plastic deformation occurs at this level of lateral displacement and increases gradually with the increase of drift ratio. The thickness of CFRP has significant influence on the maximum energy dissipation capacity of CFRP-retrofitted columns (see Fig. 7(b)). For example, the energy dissipation of the AR-1 and AR-3 columns at ultimate lateral displacement excursion, corresponding to the lateral load dropped more than 20% of the peak value, were 136.83 kN×mm and 477.79 kN×mm, respectively, the former dropped about 71.36%. From Fig. 7(b), we also observed that the column with larger longitudinal reinforcement ratio will result in larger energy dissipation capacity at the same lateral displacement and ultimate drift ratio. For example, at the drift ratio of 0.5%, the energy dissipation values of columns AR-1 and CR-1 were 25.58 kN×mm and 44.71 kN×mm, respectively, and reached 136.83 kN×mm and 545.76 kN×mm at the ultimate displacement, the former dropped about 74.93%. This is due to the increase of the CFRP volume ratio and reinforcement ratio will result in the higher available ductility that absorbed more energy. The comparisons between specimens BR-1 and BP-1, CR-1 and CP-1(see Fig. 7(a)) show that the dissipated energy of the retrofitted columns are lower than that evaluated for the repaired ones at the same drift. For example, at the drift ratio of 1%, the energy dissipation values of columns BP-1 and CP-1 were 112.23 kN×mm and 125.97 kN×mm, respectively, and 18.4% to 32.9% higher than the corresponding retrofitted columns. This might reflects that larger plastic hinge zone, more cracking and plastic deformation in the repaired columns form than that in the strengthened columns, and absorb more energy.

3.4 Stiffness degradation

The mean value of stiffness at *j*th level of ductility displacement has been evaluated by the following ratio

$$K_j = \sum_{i=1}^{n}\left(\left|+F_{ji}\right|+\left|-F_{ji}\right|\right) / \sum_{i=1}^{n}\left(\left|+\Delta_{ji}\right|+\left|-\Delta_{ji}\right|\right) \tag{1}$$

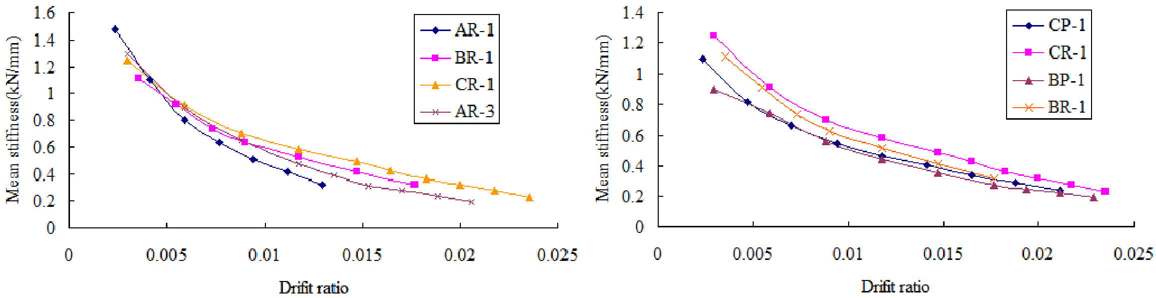

(a) (b)

Fig. 8 Comparison of the stiffness degradation versus drift ratio envelopes

where $+F_{ji}$ and $+\Delta_{ji}$ are the peak load and corresponding displacement of ith cycle at jth level of the lateral displacement in push direction respectively, and $-F_{ji}$ and $-\Delta_{ji}$ are the corresponding values in pull direction.

The relationships between K_j and the drift ratio for all of the tested columns are plotted in Fig. 8. From these curves, it can be seen that all the columns have similar stiffness degradation. Fig. 8(a) shows that the retrofitted column AR-1 deteriorates faster in terms of stiffness than the retrofitted columns AR-3. The comparison among the curves reported in Fig. 8(a) also indicates that the columns reinforced with lower longitudinal reinforcement ratio exhibit progressive stiffness degradation which is higher than those reinforced with steel rebar in larger diameter. This is reasonable because more serious deterioration occurred in the compression zone of the retrofitted columns with lower CFRP and longitudinal reinforcement ratios after the onset of the peak strength as compared with columns with higher CFRP and steel rebar volume ratios. Fig. 8(b) demonstrates that the stiffness degradation are generally similar in both the retrofitted and repaired columns in the complete displacement range, however, the retrofitted columns will result in higher mean stiffness at the same drift ratio. This is due to that the CFRP is effective in confining the concrete and maintaining the integrity of the columns, and the initial damage accelerates the concrete degradation compared with the retrofitted columns in the descending branch of the response curves.

3.5 Plastic hinge

Plastic hinge behaviour of the specimen is a critical aspect of the behaviour of RC columns under lateral cyclic loading. In many previous experimental studies, the length of plastic hinge were established based on visual observation. For example, Bae and Bayrak (2008) reported that the increase of the axial load level results in an increase in the length of the plastic hinge region, Pam and Ho (2009) concluded the plastic hinge lengths of conventional columns increase with the increase of the concrete strength. Ozbakkaloglu and Saatcioglu (2006, 2007) presented an approach based on the relationship between the lateral expansion of FRP and the level of damage sustained by concrete inside of the FRP. Idris and Ozbakkaloglu (2013) investigated the fiber type slightly influences on the plastic hinge length, showing the corner radius to section dimension ratio has no significant influence on the plastic hinge region length of the column.

In this study, based on the visual observation, the plastic hinge of CR-1 column is longer than other columns', it indicates that the longitudinal reinforcement ratio significantly influences the length of plastic hinge. Comparison of the other specimen indicates that the number of FRP layers and initial damage of the columns slightly affect the plastic hinge length of FRP-confined concrete columns within the limits of this paper.

4. Numerical approach

For implementing a finite element analysis of FRP-confined damaged rectangular or square RC columns, a fiber element model was adopted. The fiber element model was incorporated into an object-oriented non-linear finite element analysis (FEA) program, Open System for Earthquake Engineering Simulation (OpenSees). The specimens were all divided into 8 elements of equal length, three integral points were set for every element, and the discretized cross section at different integral points consisted of confined concrete and internal steel reinforcement. Each component in the section was modeled with a different material model in OpenSees.

4.1 Material model

The confinement model of Lam and Teng (2003) was selected as the backbone curve for the core concrete material, and cast into the concrete model of Kent-Park-Scott (Scott *et al*. 1982, Taucer *et al*. 1991), which is built into OpenSees with hysteretic features. The stress-strain relation for FRP-confined concrete proposed by Lam and Teng (2003) is as follows

$$\begin{cases} \sigma_{\mathrm{c}} = E_{\mathrm{c}}\varepsilon_{\mathrm{c}} - \dfrac{\left(E_{\mathrm{c}} - E_2\right)^2}{4f_{\mathrm{c0}}^{'}}\varepsilon_{\mathrm{c}}^2 & 0 \le \varepsilon_{\mathrm{c}} \le \varepsilon_{\mathrm{t}} \\ \sigma_{\mathrm{c}} = f_{\mathrm{c0}}^{'} + E_2\varepsilon_{\mathrm{c}} & \varepsilon_{\mathrm{t}} \le \varepsilon_{\mathrm{c}} \le \varepsilon_{\mathrm{cc}} \end{cases} \tag{2}$$

where E_{c} and $f_{\mathrm{c0}}^{'}$ are the initial elastic modulus and the initial compressive strength of the unconfined concrete, E_2 is the slope of the linear second portion, ε_{t} is the strain of the smooth transition of the parabolic first portion meeting the linear second portion, and $\varepsilon_{\mathrm{cc}}$ is the ultimate strain of the confined damaged concrete and can be derived to

$$\varepsilon_{\mathrm{cc}} = \left(\frac{2f_{\mathrm{c0}}^{'}}{E_{\mathrm{c}}}\right)\cdot\left(1.75 + 12\left(\frac{f_{\mathrm{l}}}{f_{\mathrm{c0}}^{'}}\right)\left(\frac{\varepsilon_{\mathrm{h,rup}}E_{\mathrm{c}}}{2f_{\mathrm{c0}}^{'}}\right)^{0.45}\right) \tag{3}$$

where $\varepsilon_{\mathrm{h,rup}}$ is the FRP hoop strain at rupture, selected as $0.686\varepsilon_{\mathrm{f}}$ for carbon-FRP (Lim and Ozbakkaloglu 2013, 2015) in this study, ε_{f} is the FRP material ultimate tensile strain, and f_{l} is the actual maximum confining pressure, for the FRP-C RC columns with rectangular section, given by

$$f_{\mathrm{lr}} = \frac{b}{h}\frac{1-\left(\left((b/h)\left(h-2R_{\mathrm{c}}\right)^2 + (h/b)\left(b-2R_{\mathrm{c}}\right)^2\right)/\left(3A_{\mathrm{g}}\right)\right)-\rho}{1-\rho}\cdot\frac{2E_{\mathrm{f}}t_{\mathrm{f}}\varepsilon_{\mathrm{f}}}{\sqrt{h^2+b^2}} \tag{4}$$

where E_{f} and t_{f} are the elastic modulus and thickness of the FRP, respectively, b and h are the width and depth of the cross section, R_c is the corner radius of the cross section, ρ is the longitudinal reinforcement ratio, and A_g is the sectional area.

To accurately predict the initial state and simulate the hysteretic behavior of CFRP-C DSRC columns, it is necessary to add the initial damage into the constitutive model for confined concrete and simulate the damage process mathematically by the damage constitutive model. In this paper, the damage indicator D in terms of concrete compressive strain from reference (Qian and Zhou 1989) was selected to quantify the damage of RC members, which can be denoted as

$$\begin{cases} D=0 & 0\le\varepsilon\le\varepsilon_{\mathrm{f}} \\ D=\dfrac{\varepsilon-\varepsilon_{\mathrm{f}}}{\varepsilon_{\mathrm{u}}-\varepsilon_{\mathrm{f}}}\dfrac{\varepsilon_{\mathrm{u}}}{\varepsilon} & \varepsilon_{\mathrm{f}}\le\varepsilon\le\varepsilon_{\mathrm{u}} \end{cases} \tag{5}$$

where ε is the concrete compressive strain, ε_{f} is the concrete compressive peak strain, and ε_{u} is the concrete compressive ultimate strain.

At every converged step, the element response was fed into the damage model, and the damage index at the element level was calculated directly from the strain at a Gauss integral calculus point. The recorded damage indices of overall elements were used for updating the constitutive parameters of the concrete by the elastic modulus reduction

$$E_i^{\mathrm{d}}=(1-D_i)E_i \qquad i=1\sim n \tag{6}$$

where D_i is the damage indicator of the ith element, E_i and E_i^{d} are the elastic modulus of the ith undamaged concrete element and the effective elastic modulus of the ith damaged concrete element, respectively.

The hysteretic behavior of the steel reinforcement in CFRP-C (D)SRC columns can be simulated using the non-linear constitutive model of Giuffre-Menegotto-Pinto (Filippou *et al.* 1983). The elastic and yield asymptotes in this model were assumed to be straight lines, and the unloading slope remains constant and equals to the initial slope. More details about the definition of cyclic parameters can be found in reference (Filippou *et al.* 1983).

4.2 Numerical results

We compared the results of the FEA method with test data for the repaired columns BP-1, CP-1, and the retrofitted columns AR-1, AR-3, BR-1 and CR-1 respectively, see Fig. 9. It is observed that, in general, there is a good agreement between the numerical and experimental results in terms of the stiffness, load capacity, and the ultimate point.

The slight discrepancy for the calculated results is observed primarily in the little smaller areas enclosed by the hysteretic loops and a slightly higher peak horizontal load carrying capacity. This may be attributed to the numerical model assumes perfect bond between concrete and CFRP, and neglects creep of CFRP and creep and shrinkage of concrete for the short-term cyclic loading. However, if the ultimate displacement is defined as the lateral displacement corresponding to the point where the horizontal load carrying capacity drops to 85% of the peak capacity, the ductility predicted by the analysis is close to the actual ductility achieved by the test specimens, as shown in Fig. 9.

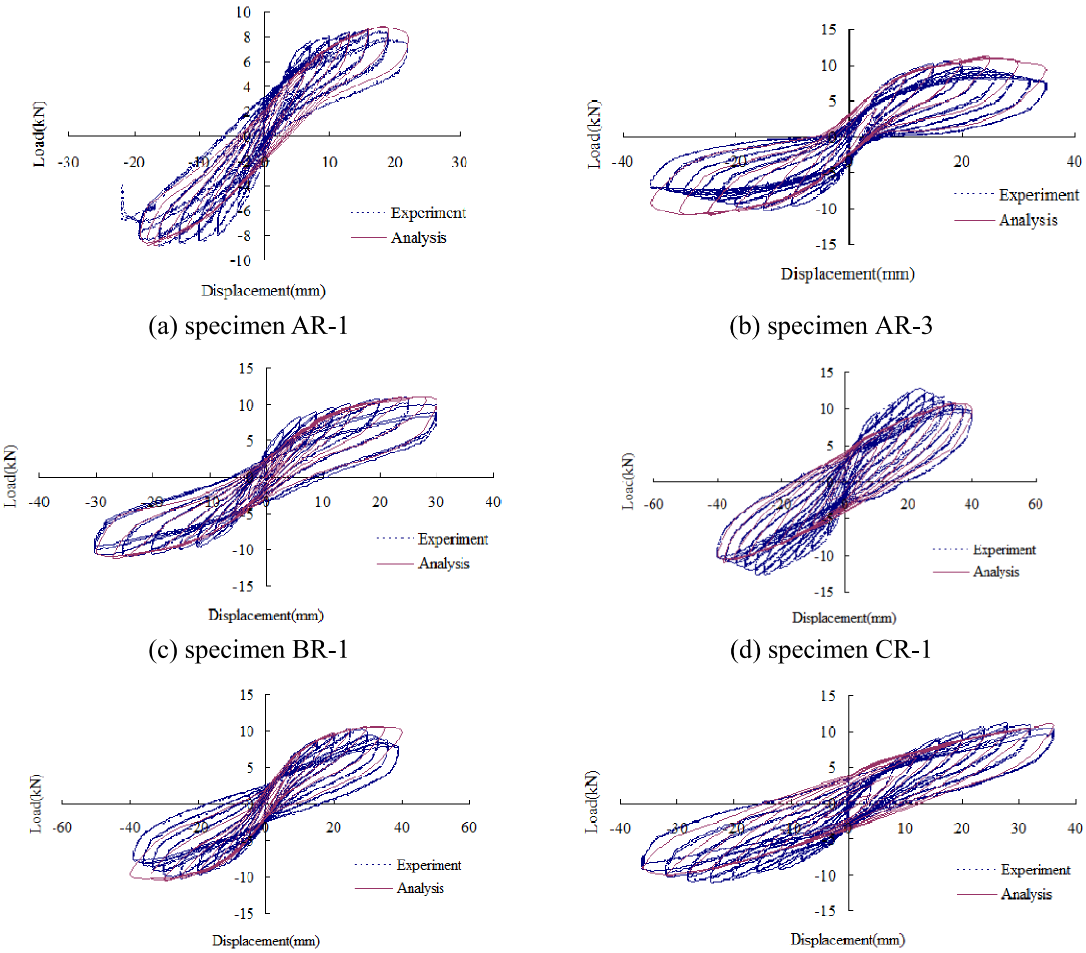

(a) specimen AR-1 (b) specimen AR-3

(c) specimen BR-1 (d) specimen CR-1

(e) specimen BDP-1 (f) specimen CDP-1

Fig. 9 Comparison of test data and numerical results for hysteretic response of retrofitted and repaired columns

5. Conclusions

The effects of initial damage, the amount of confining CFRP and longitudinal reinforcement ratio on the cyclic behavior of CFRP-C (D)SRC columns were investigated in this study. Using the developed confinement models taking initial damage into consideration, a numerical study was further carried out on CFRP-C (D)SRC columns. The following conclusions may be drawn from this study:

- CFRP composite wraps are effective in restoring the flexural strength and ductility capacity of strengthened and repaired columns, and the cyclic behavior and energy dissipation capacity of CFRP-C (D)SRC columns progressively improve through decrease in stiffness and strength degradation rates as the number of CFRP layers increase.
- After repairing with CFRP wrap, columns with larger reinforcement ratio develop stable

hysteresis loops and higher lateral resistance, and show weak sign of stiffness and energy dissipation degradation. For example, the reinforcement ratio changed from 0.792 to 2.567, the increase of the flexural strength and energy dissipation up to ultimate drift were 4.09 kN and 74.93%;

- In all repaired specimens, the rate of stiffness deterioration and energy dissipation under large reversed cyclic loading are higher than that of the corresponding retrofitted columns. However, the initial stiffness and maximum lateral resistance of the repaired columns are lower than that of the strengthened columns;
- Comparison of the numerical and test results indicates that the numerical analysis provides a rational explanation and prediction to the behavior of the strengthened and repaired CFRP-confined columns.

Acknowledgments

This work was supported by the National Natural Science Foundation of China (51278038) and the Doctorial Innovation Fund of Beijing Jiaotong University (C13JB00180).

References

Bae, S. and Bayrak, O. (2008), "Plastic hinge length of reinforced concrete columns", *ACI Struct. J.*, **105**(3), 290-300.

Biskinis, D. and Fardis, M.N. (2013), "Models for FRP-wrapped rectangular RC columns with continuous or lap-spliced bars under cyclic lateral loading", *Eng. Struct.*, **57**, 199-212.

Cheng, C.T., Yang, J.C., Yeh, Y.K. and Chen, S.E. (2003), "Seismic performance of repaired hollow-bridge piers", *Constr. Build. Mater.*, **17**(5), 339-351.

Filippou, F.C., Popov, E.P. and Bertero, V.V. (1983), *Effects of Bond Deterioration on Hysteretic Behavior of Reinforced Concrete Joints*, Report No. EERC 83-19; Earthquake Engineering Research Center, Berkeley, CA, USA.

Galal, K., Arafa, A. and Ghobarah, A. (2005), "Retrofit of RC square short columns", *Eng. Struct.*, **27**(5), 801-813.

Haroun, M. and Elsanadedy, H. (2005), "Behavior of cyclically loaded squat reinforced concrete bridge columns upgraded with advanced composite-material jackets", *J. Bridge Eng.*, **10**(6), 741-748.

Iacobucci, R.D., Sheikh, S.A. and Bayrak, O. (2003), "Retrofit of square concrete columns with carbon fiber-reinforced polymer for seismic resistance", *ACI Struct. J.*, **100**(6), 785-794.

Idris, Y. and Ozbakkaloglu, T. (2013), "Seismic behavior of high-strength concrete-filled FRP tube columns", *J. Compos. Constr.*, **17**(6), 04013013.

Lam, L. and Teng, J.G. (2003), "Design-oriented stress–strain model for FRP-confined concrete", *Constr. Build. Mater.*, **17**(6), 471-489.

Li, X.R., Wang, Y.F. and Su, L. (2014), "Damping determination of FRP-confined reinforced concrete columns", *Comput. Concrete*, **14**(2), 163-174.

Lim, J.C. and Ozbakkaloglu, Y. (2013), "Confinement model for FRP-confined high-strength concrete", *J. Compos. Constr.*, **18**(4), 04013058.

Lim, J.C. and Ozbakkaloglu, Y. (2015), "Hoop strains in FRP-confined concrete columns: Experimental observations", *Mater. Struct.*, **48**(9), 2839-2854.

Ozbakkaloglu, T. and Saatcioglu, M. (2006), "Seismic behavior of high strength concrete columns confined by fiber-reinforced polymer tubes", *J. Compos. Constr.*, **10**(6), 538-549.

Ozbakkaloglu, T. and Saatcioglu, M. (2007), "Seismic performance of square high-strength concrete columns in FRP stay-in-place formwork", *J. Struct. Eng.*, **133**(1), 44-56.

Pam, H.J. and Ho, J.C.M. (2009), "Length of critical region for confinement steel in limited ductility high-strength reinforced concrete columns", *Eng. Struct.*, **31**(12), 2896-2908.
Qian, J.C. and Zhou, J.F. (1989), "Two concrete damage model and their application", *J. Hohai Univ.*, **17**(3), 40-47.
Realfonzo, R. and Napoli, A. (2009), "Cyclic behavior of RC columns strengthened by FRP and steel devices", *J. Struct. Eng.*, **135**(10), 1164-1176.
Saadatmanesh, H., Ehsani, M.R. and Jin, L. (1997), "Repair of earthquake-damaged RC columns with FRP wraps", *ACI Struct. J.*, **94**(2), 206-215.
Saiidi, M. and Cheng, Z. (2004), "Effectiveness of composites in earthquake damage repair of reinforced concrete flared columns", *J. Compos. Constr.*, **8**(4), 306-314.
Scott, B.D., Park, R. and Priestley, M.J.N. (1982), "Stress-strain behavior of concrete confined by overlapping hoops at low and high strain rates", *ACI Struct. J.*, **79**(1), 13-27.
Sheikh, S.A. and Yau, G. (2002), "Seismic behavior of concrete columns confined with steel and fiber-reinforced polymers", *ACI Struct. J.*, **99**(1), 72-80.
Taucer, F., Spacone, E. and Filippou, F.C. (1991), *A Fiber Beam-column Element for Seismic Response Analysis of Reinforced Concrete Structures*, (Vol. 91, No. 17), Earthquake Engineering Research Center, College of Engineering, University of California, Berkeley, CA, USA.
Wang, Y.F. and Li, X.R. (2013), "Non-linear damping of FRP-confined damaged reinforced concrete columns", *Eng. Struct.*, **57**, 289-295.
Wu, Y., Liu, T. and Wang, L. (2008), "Experimental investigation on seismic retrofitting of square RC columns by carbon FRP sheet confinement combined with transverse short glass FRP bars in bored holes", *J. Compos. Constr.*, **12**(1), 53-60.
Xiao, Y. and Ma, R. (1997), "Seismic retrofit of RC circular columns using prefabricated composite jacketing", *J. Struct. Eng.*, **123**(10), 1357-1364.
Ye, L.P., Zhang, K., Zhao, S.H. and Feng, P. (2003), "Experimental study on seismic strengthening of RC columns with wrapped CFRP sheets", *Constr. Build. Mater.*, **17**(6), 499-506.

CC